Electronic Supplementary Material (ESI) for Physical Chemistry Chemical Physics.

Supplementary Information

The Photochemistry and Photophysics of Benzoyl-Carbazole

Yinon Deree, [a] Benny Bogoslavsky,[a] Igor Schapiro*[b] and Ori Gidron* [a]

[a] Institute of Chemistry and the Center for Nano science and Nano-technology, The Hebrew University of Jerusalem Edmond J. Safra Campus, 9190401 Jerusalem, Israel E-mail: ori.gidron@mail.huji.ac.il

[b] Fritz Haber Center for Molecular Dynamics, Institute of Chemistry, The Hebrew University of Jerusalem, Jerusalem, Israel. E-mail: igor.schapiro@mail.huji.ac.il

Contents

S1 General 3
S2 Synthesis of c-F_4BCz 4
S3 Crystal Data for c-F_4BCz 6
S4 Characterization of the Photoproducts for BCz 7
S5 Photophysical properties 9
S6 TADF kinetic model 16
S7 Photochemical kinetics 20
S8 Calculations 21

S1 General

Carbazole was purchased from Alfa Aesar and purified using HPLC (Chiralpak-IB, 1:9 EtOAc:Hexane). Benzoyl chloride, pentafluorobenzoyl chloride, and 4-fluorobenzoyl chloride were purchased from Apollo Scientific. Compounds **BCz**, **F_5BCz** and o-**F_1BCz** were synthesized according to a previous report[1]. Flash chromatography (FC) was performed using CombiFlash SiO_2 columns. 1H and 13C NMR spectra were recorded in solution on a Bruker-AVIII 400 MHz and 500 MHz spectrometers using tetramethylsilane (TMS) as the external standard. The spectra were recorded using chloroform-d as the solvent. Chemical shifts are expressed in δ units. UV-vis absorption spectra were recorded with an Agilent Cary-5000 spectrophotometer. The spectra were measured using a quartz cuvette (1 cm) at 25 °C. The absorption wavelengths are reported in nm with the extinction coefficient ε (M^{-1} cm^{-1}) in brackets. Steady-state fluorescence measurements were performed on a HORIBA JOBIN YVON Fluoromax-4 spectrofluorometer with the excitation/emission geometry at right angles. Fluorescence quantum yields (ϕf) were determined using a standard procedure under a HORIBA- Φ integrating sphere. The lifetimes of the excited species were measured using an NL-C2 Pulsed Diode Controller NanoLED light source with time-correlated single photon counting (TSCPC) Controller DeltaHub (HORIBA), referenced against colloidal Ludox solution (50 wt. % solution in water) obtained from Aldrich. High-resolution mass spectra were measured on Dionex UltiMate 3000 UPLC (Thermo Fisher Scientific).

S2 Synthesis of c-F_4BCz

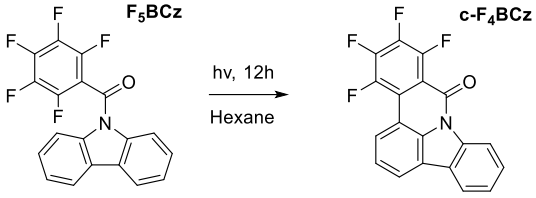

A solution of **F_5BCz** (0.135 g) in hexane (300 ml) was placed in a photochemical cell (PhotoRedox Box, HepatoChem) and irradiated under 350 nm for 12 hr until full conversion of **F_5BCz** (monitored by TLC). The resulting product was dried ($MgSO_4$), evaporated, and separated using silica gel chromatography using ethyl acetate/hexane (1:9) to afford light-yellow solid (50 mg, 40% yield). HRMS (ESI) calculated for $C_{19}H_8F_4NO$ 342.05365, found 342.05316 $(M+H)^+$.

^{1}H-NMR (500 MHz, $CDCl_3$) δ 8.71 (d, J = 8.2 Hz, 1H, H-C(10)), 8.38 (d, J = 8.0 Hz, 1H, H-C(13)), 8.08 (d, J = 7.6 Hz, 1H, H-C(1)), 8.01 (dt, J = 7.7, 1.0 Hz, 1H, H-C(3)), 7.59 – 7.52 (m, 2H, H-C(2), H-(C12)), 7.47 (td, J = 7.6, 1.1 Hz, 1H, H-C(11)). ^{13}C-NMR (126 MHz, $CDCl_3$) δ 155.36 (C16), 137.99 (C17,20), 133.69 (C18,19), 128.64 (C12), 126.05 (C8), 125.72 (C11), 125.27 (C4), 125.10 (C13), 125.02 (C2), 125.04 (C5), 124.52, 122.60 (C1), 120.81 (C3),120.2 (C7), 117.63 (C10), 113.06 (C14), 112.53 (C15).

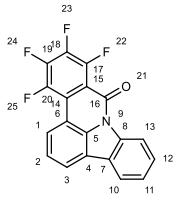

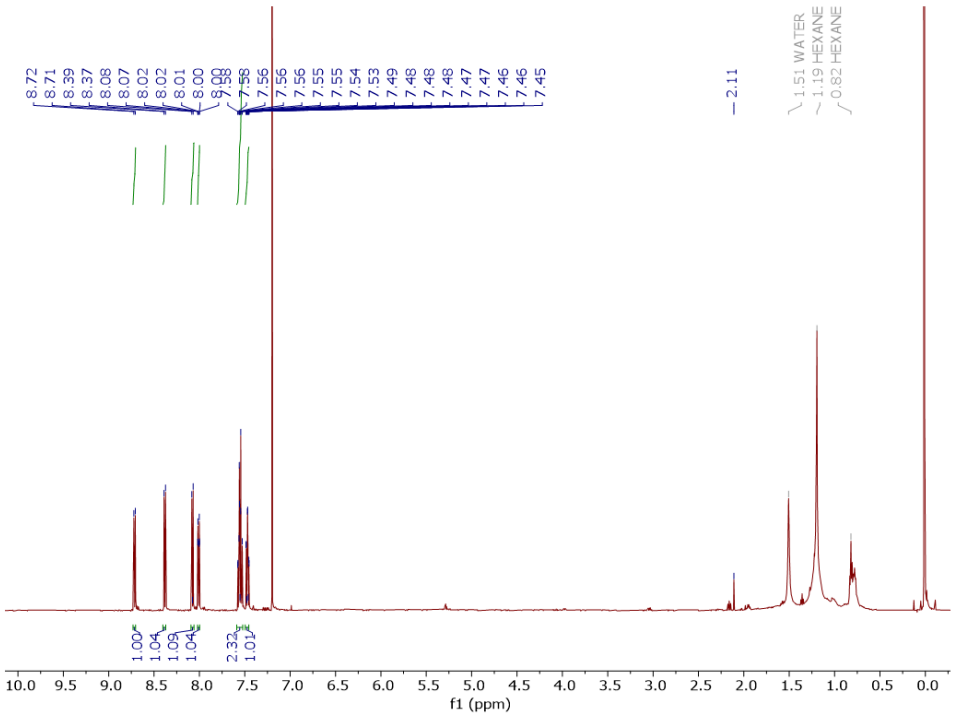

Figure S1. ^{1}H NMR (400 MHz) of **c-F_4BCz** in CDCl3, measured at 298 K.

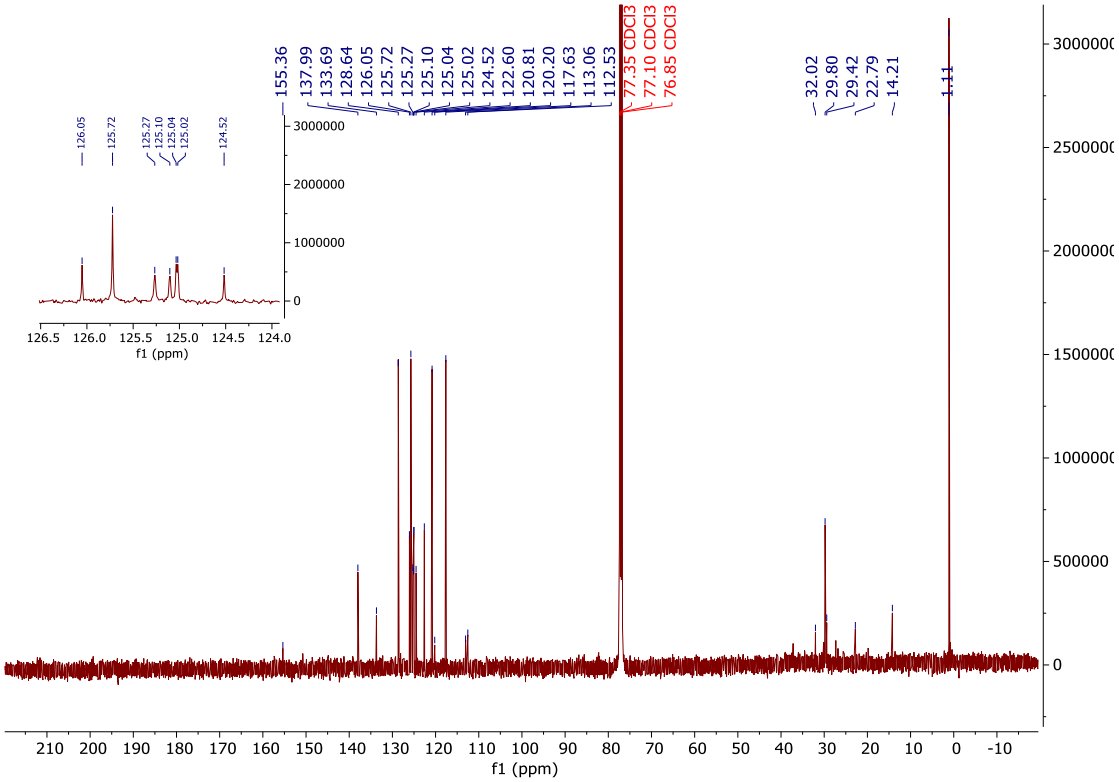

Figure S2. ^{13}C-NMR (400 MHz) of **c-F$_4$BCz** in $CDCl_3$, measured at 298 K.

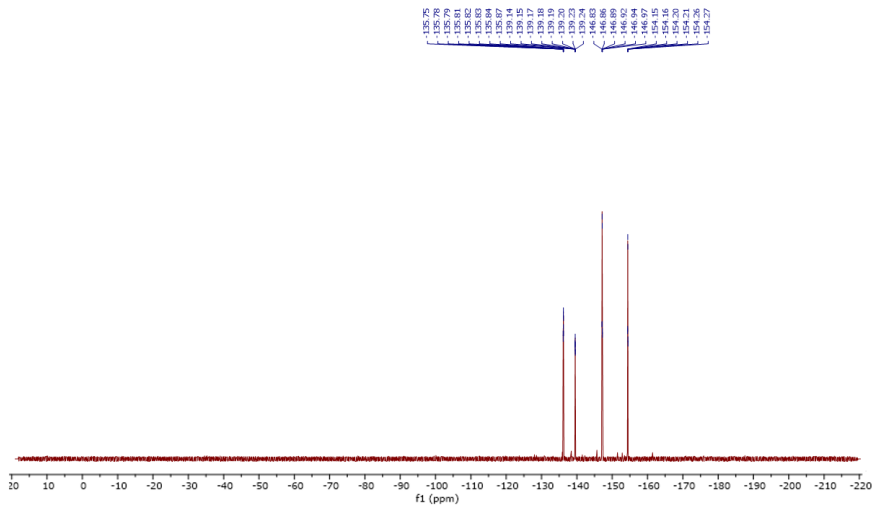

Figure S3. ^{19}F-NMR (400 MHz) of **c-F$_4$BCz** in $CDCl_3$, measured at 298 K.

S3 Crystal Data for c-F_4BCz

CCDC Number	2352149
Empirical formula	$C_{19}H_7F_4NO$
Formula weight	341.26
Temperature/K	100.0 (1)
Crystal system	monoclinic
Space group	$P2_1/n$
a/Å	6.9645(3)
b/Å	13.1363(6)
c/Å	14.5331(6)
α/°	90
β/°	93.668(4)
γ/°	90
Volume/Å^3	1326.9(1)
Z	4
ρ_{calc}g/cm^3	1.708
μ/mm^{-1}	0.145
F(000)	688.0
Crystal size/mm^3	0.322 × 0.058 × 0.038
Radiation	Mo Kα (λ = 0.71073)
2Θ range for data collection/°	6.202 to 64.056
Index ranges	$-8 \leq h \leq 9$, $-18 \leq k \leq 13$, $-20 \leq l \leq 19$
Reflections collected	8943
Independent reflections	3721 [R_{int} = 0.0372, R_{sigma} = 0.0535]
Data/restraints/parameters	3721/0/226
Goodness-of-fit on F^2	1.038
Final R indexes [I>=2σ (I)]	R_1 = 0.0720, wR_2 = 0.1617
Final R indexes [all data]	R_1 = 0.1142, wR_2 = 0.1806
Largest diff. peak/hole / e Å^{-3}	0.53/-0.30

S4 Characterization of the Photoproducts for BCz

A solution of **BCz** hexane was placed in the photochemical cell (PhotoRedox Box, HepatoChem) and irradiated under 350 nm for 12 hr. The resulting product was dried ($MgSO_4$), evaporated, and separated using silica gel chromatography using ethyl acetate/hexane (1:9). Carbazole and the 1,3-rearrangment products were isolated in small quantities and verified using literature data.[2]

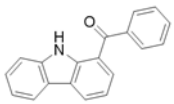

^{1}H-NMR (400 MHz, $CDCl_3$) δ 10.55 (s, 1H), 8.33 (ddd, J = 7.6, 1.1, 0.7 Hz, 1H), 8.14 (ddt, J = 7.9, 1.4, 0.8 Hz, 1H), 7.83 – 7.78 (m, 3H), 7.64 – 7.48 (m, 5H), 7.34 – 7.29 (m, 1H), 7.28 – 7.23 (m, 1H).

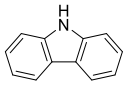

^{1}H NMR (400 MHz, $CDCl_3$) δ 8.09 (dd, J = 7.8, 0.9 Hz, 2H), 7.46 – 7.38 (m, 4H), 7.28 – 7.22 (m, 2H).

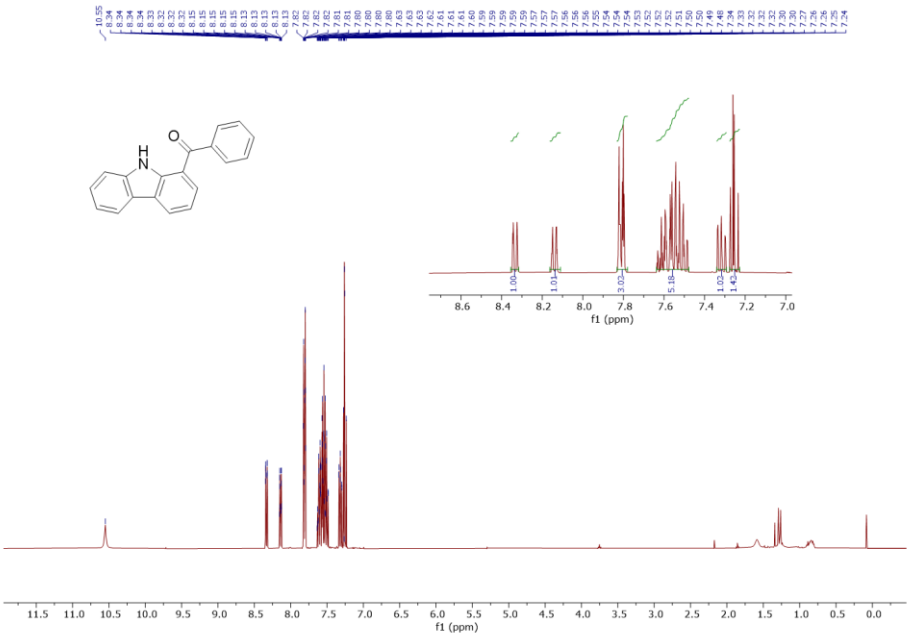

Figure S4. ^{1}H NMR (400 MHz) of the 1,3-rearrngment product of **BCz** in $CDCl_3$, measured at 298 K.

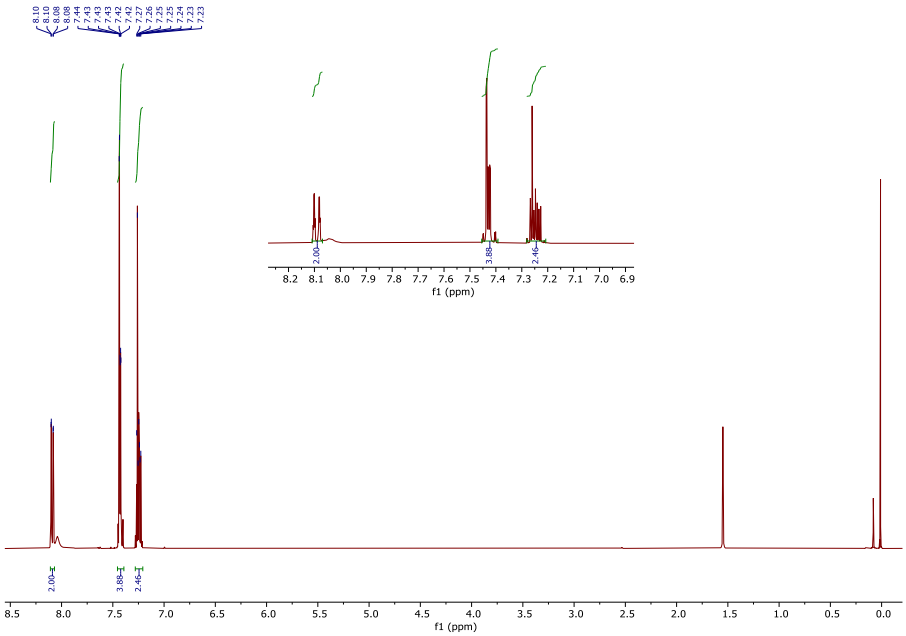

Figure S5. ^{1}H NMR (400 MHz) of carbazole (isolated from the photoreaction of **BCz**) in CDCl3, measured at 298 K.

S5 Photophysical properties

All spectra where recorded in low OD (0.05 max) to avoid self-absorption effect/inner filter effect.

Solution λ_{max}		Solid λ_{max}	
BCz	**F_5BCz**	**BCz**	**F_5BCz**
278nm	276nm	277nm	286nm
305nm	299nm	300nm	302nm
315nm	311nm	312nm	319nm

Table S1. λ_{max} of absorption for 1 and 2.

Name	Φ_F	τ (ns)
BCz	~0%	1.4
F_5BCz	10%	3

Table S2. Solid state photophysical properties.

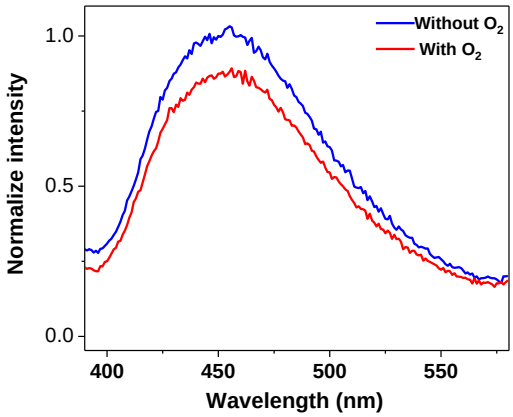

Figure S6. Fluorescence spectra of **BCz** in Hexane with oxygen (red) and without (blue). The integration ratio of is 0.9.

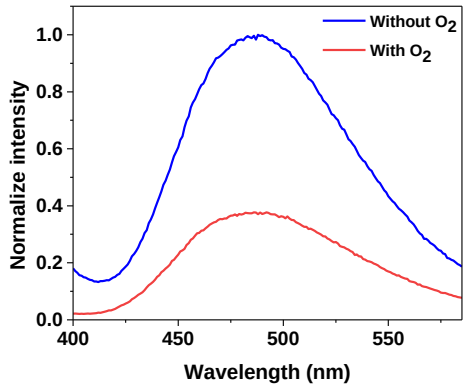

Figure S7. Fluorescence spectra of **BCz** in toluene with oxygen (red) and without (blue). The integration ratio is 0.4.

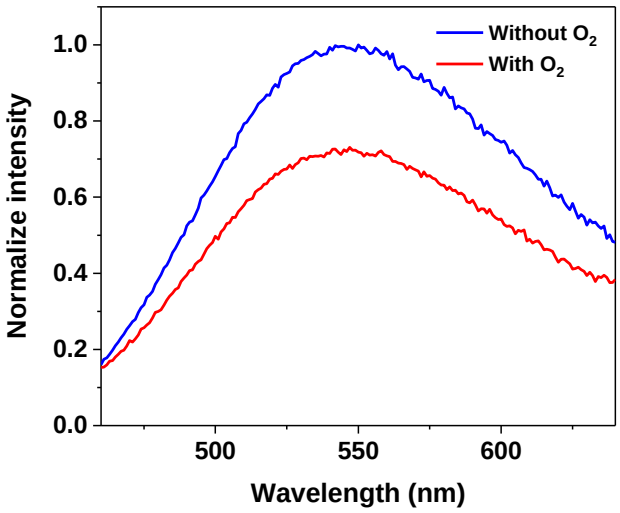

Figure S8. Fluorescence spectra of **BCz** in acetonitrile with oxygen (red) and without (blue). The integration ratio is 0.7.

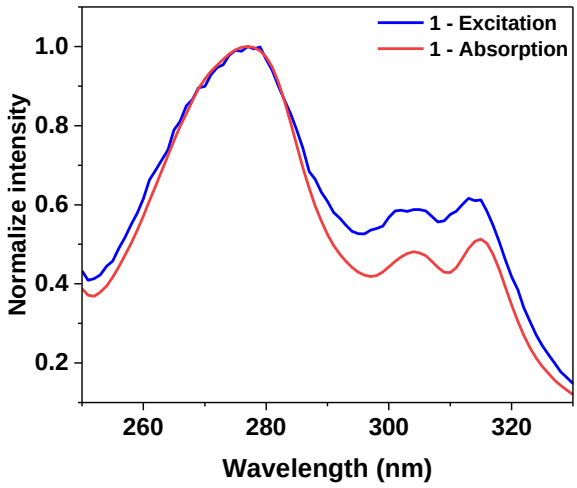

Figure S9. Excitation (450 nm) and absorption spectra of **BCz** in hexane.

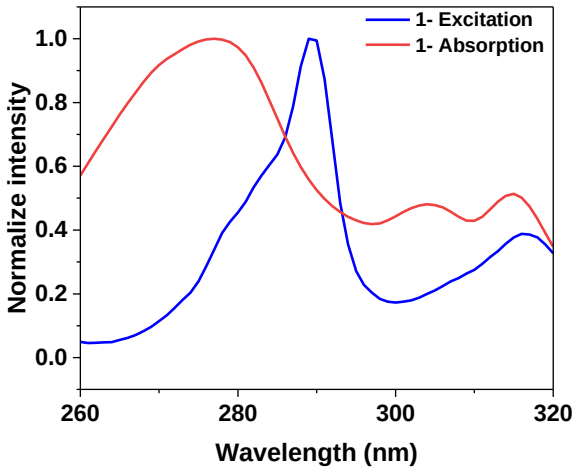

Figure S10. Excitation (350 nm) and absorption spectra of **BCz** in hexane.

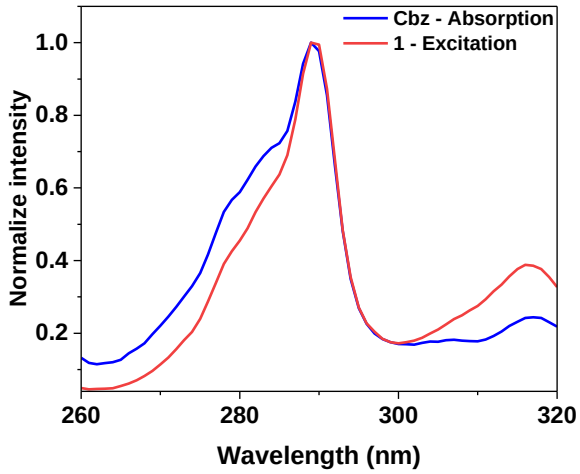

Figure S11. Excitation (350 nm) of **BCz** and absorption spectra of carbazole in hexane.

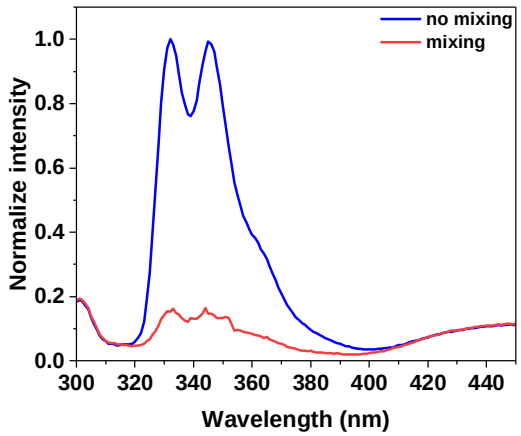

Figure S12. Measuring **BCz** with the same OD with and without mixing in hexane. If the signal in 350 nm originates from a photoreaction, the intensity is expected to decrease relative to the non-mixing conditions since the photoproducts formed in the area of the excitation beam. When mixing, the photoproducts will disperse uniformly in the solution faster. Thus, their concentration inside the beam will be lower (only molecules inside the beam are responsible for the emission signal).

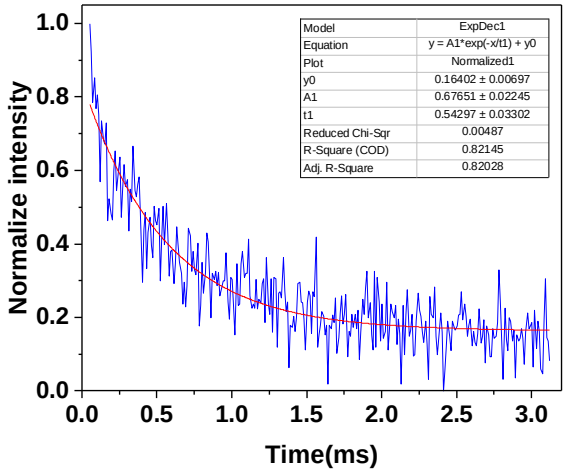

Figure S13. Phosphorescence lifetime of **BCz** (solid state at 77 K), emission peak 472 nm.

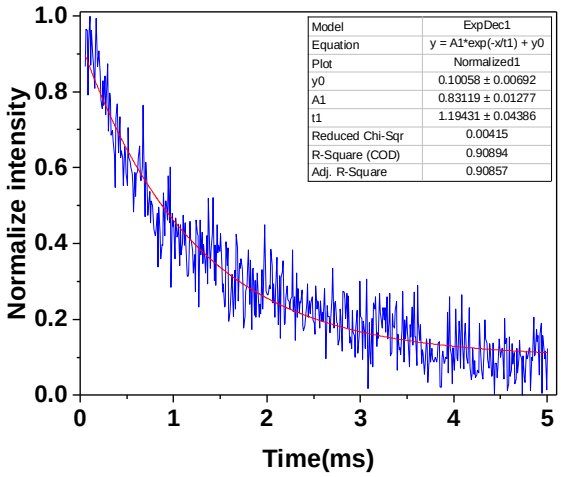

Figure S14. Phosphorescence lifetime of **F_5BCz** (solid state at 77 K), emission peak 500 nm.

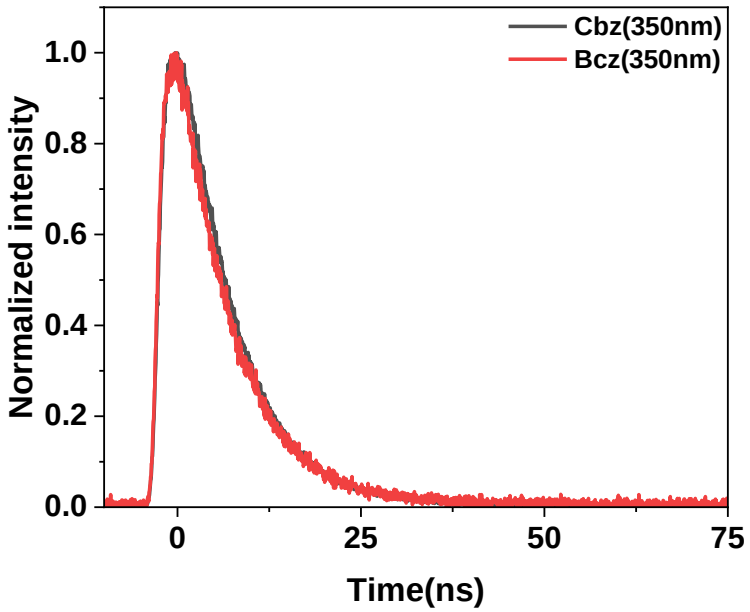

Figure S14B. Fluorescence lifetime of the 350 nm peak of **BCz** and carbazole in hexane. The measured lifetime was fitted to one exponent with a value of 6.5 ns for both.

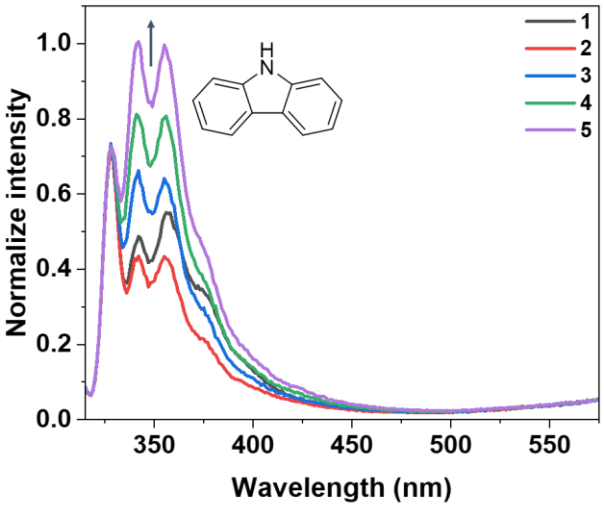

Figure S15. Emission spectra of **F_5BCz** in tetrahydrofuran solution as a function of number of measurements. It is clear to see that compound **c-F_4BCz** is not forming like as observed when hexane was used as a solvent. However, the emergence of carbazole does peak is an indication of the photo-Fries rearrangement. The peak as 325 nm is the of the solvent Raman peak.

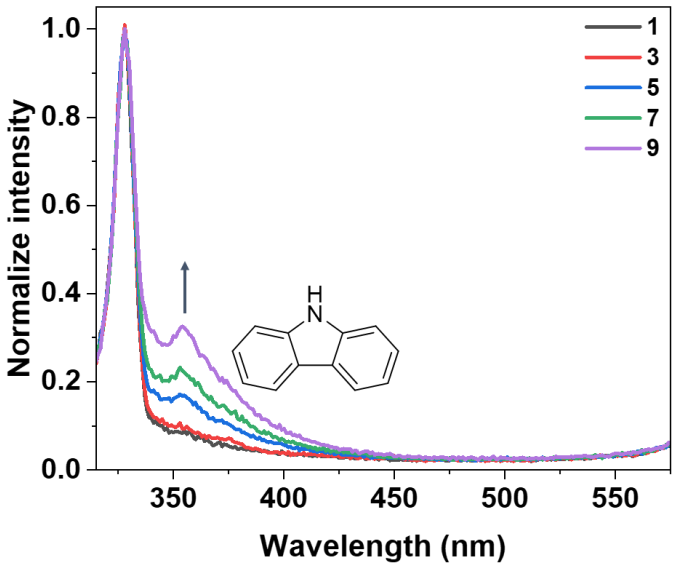

Figure S16. Emission spectra of **F_5BCz** in acetonitrile solution as a function of number of measurements.

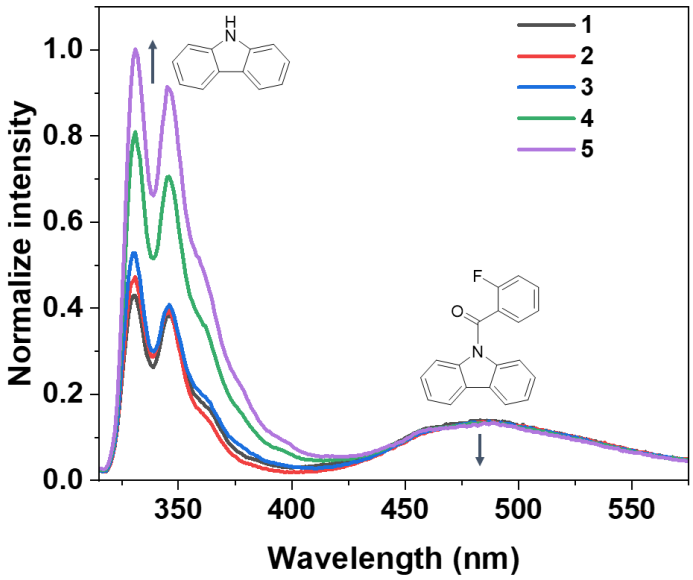

Figure S17. Emission spectra of o-**F_1BCz** in hexane solution as a function of number of measurements. The cyclization photoreaction does not take place, since there is no emission signal in the 350nm-450nm (the photo cyclization product of o-**F_1BCz** and **F_5BCz** should emit in the same region since fluorine atoms has little effect in emission of aromatic rings).

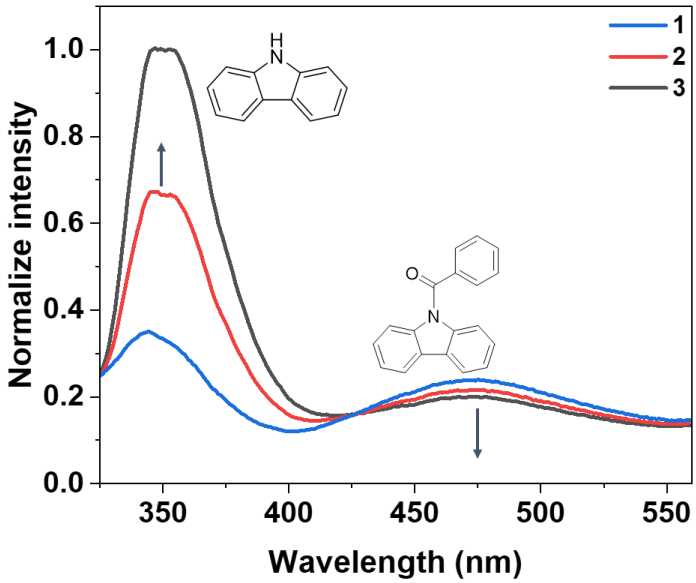

Figure S18. Emission spectra of **BCz** in PMMA matrix as a function of number of measurements. The film was formed by dissolving 5 mg of **BCz** in saturated PMMA solution in 35ml of toluene followed by drop casting on a quartz slide.

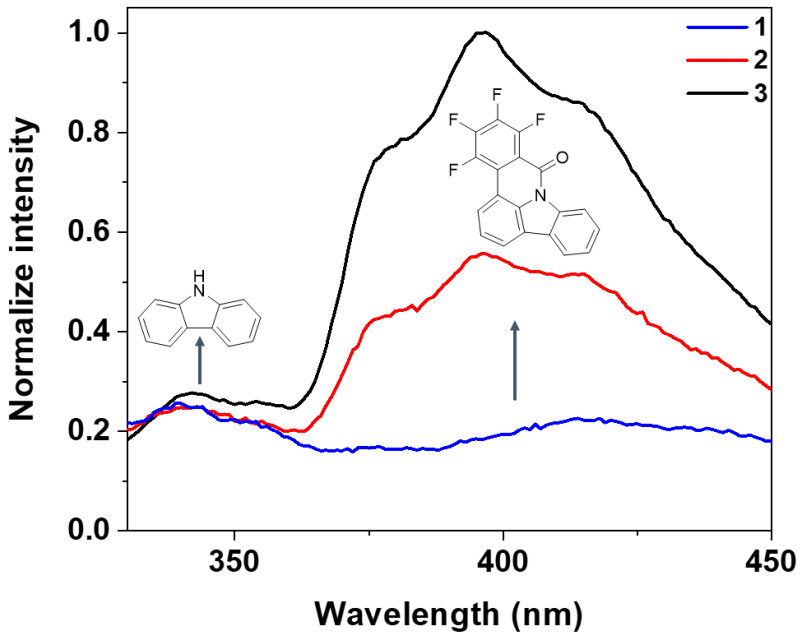

Figure S19. Emission spectra of **F_5BCz** in PMMA matrix as a function of the number of measurements.

S6 TADF kinetic model

To explain the experimental lifetime measurements of **BCz** in solution it is well excepted to model TADF with coupled differential equations[3]. The differential equations for the decay of the first excited singlet state (S_1) and the second excited triplet state (T_1) are given by:

(C1) $\frac{d[S_1(t)]}{dt} = -[S_1(t)]\left(k_f + k_{nr}^S + k_{isc}\right) + [T_1(t)]k_{risc}$

(C2) $\frac{d[T_1(t)]}{dt} = [S_1(t)]k_{isc} - [T_1(t)](k_p + k_{nr}^T + k_{risc})$

We also define:

$k_S = k_f + k_{nr}^S + k_{isc}$

$k_T = k_p + k_{nr}^T + k_{risc}$

where the decay constants for the singlet and triplet states are given by $k_S = k_f + k_{nr}^S + k_{isc}$ and $k_T = k_p + k_{nr}^T + k_{risc}$ (meaning the sum of all the rate constants of reactions that cause the decay of the S_1 state and T_1 state) ,where k_f is the fluorescence rate constant, k_{nr}^S is the rate constant for the non-radiative decay of the singlet state, k_{isc} is the rate constant for intersystem crossing, k_p is the rate constant for phosphorescence, k_{nr}^T is the rate constant for the non-radiative decay of the triplet state, and k_{risc} is the rate constant for reverse intersystem crossing.

Finally:

(C3) $\frac{d[S_1(t)]}{dt} = -k_S[S_1(t)] + k_{risc}[T_1(t)]$

(C4) $\frac{d[T_1(t)]}{dt} = k_{isc}[S_1(t)] - k_T[T_1(t)]$

The solution for the singlet functional is therefore (B_1 and B_2 are amplitudes):

(C5) $[S_1(t)] = B_1e^{a_1t} + B_2e^{a_2t}$

which is like the experimental singlet state functional, and the solution for the triplet functionality is (C_1 and C_2 are amplitudes):

(C6) $[T_1(t)] = C_1e^{a_1t} + C_2e^{a_2t}$

Using the following boundary conditions:

$[S_1(0)] = B_1 + B_2$

$0 = C_1 + C_2$

We can obtain the derivatives of equations 5 and 6:

(C7) $\frac{d[S_1(t)]}{dt} = B_1a_1e^{a_1t} + B_2a_2e^{a_2t}$

(C8) $\frac{d[T_1(t)]}{dt} = C_1a_1e^{a_1t} + C_2a_2e^{a_2t}$

Substituting equations 5 and 6 into equations 3 and 4 yields:

(C9) $\frac{d[S_1(t)]}{dt} = -(k_s)(B_1e^{a_1t} + B_2e^{a_2t}) + k_{risc}(C_1e^{a_1t} + C_2e^{a_2t})$

(C10) $\frac{d[T_1(t)]}{dt} = k_{isc}(B_1e^{a_1t} + B_2e^{a_2t}) - (k_T)(C_1e^{a_1t} + C_2e^{a_2t})$

Factoring out the exponents produces:

(C11) $\frac{d[S_1(t)]}{dt} = e^{a_1t}[-k_sB_1 + k_{risc}C_1] + e^{a_2t}[-k_sB_2 + k_{risc}C_2]$

(C12) $\frac{d[T_1(t)]}{dt} = e^{a_1t}[k_{isc}B_1 - k_TC_1] + e^{a_2t}[k_{isc}B_2 - k_TC_2]$

Comparing the coefficients of the exponents in equations 11 and 12 compared with equations 7 and 8 yields:

(C13) $-k_sB_1 + k_{risc}C_1 = B_1a_1$

(C14) $-k_sB_2 + k_{risc}C_2 = B_2a_2$

(C15) $k_{isc}B_1 - k_TC_1 = C_1a_1$

(C16) $k_{isc}B_2 - k_TC_2 = C_2a_2$

Rearrangement of this equations with the boundary conditions obtains the following equations:

(C17) $k_s = \frac{-[\frac{B_1}{B_2}a_1 + a_2]}{\frac{B_1}{B_2} + 1}$

(C18) $k_T = \frac{-\left[\frac{B_1}{B_2}a_2 + a_1\right]}{\frac{B_1}{B_2} + 1}$

(C19) $(a_1 + k_s)(a_1 + k_T) = k_{isc}k_{risc}$

The values of B_1, B_2, a_1 and a_2 can be determined experimentally by fitting the fluorescence lifetime to the form of equation 5

The function for the exponents is (can be obtained from the eigenvalues of the rate constants matrix, derivation not shown):

(C20) $a_{1,2} = \frac{-(k_S+k_T)\pm\{(k_S+k_T)^2-4(k_Sk_T-k_{isc}k_{risc})\}^{0.5}}{2}$

Thus, the lifetimes are the negative inverse of $a_{1,2}$.

This model explains three important experimentally observations:

1.Only one exponent is sensitive to oxygen (the longer one).

2.One lifetime is considerably longer than the other one.

3. The effect of oxygen on the quantum efficiency of fluorescence increases as the polarity decreases in solvents where TADF observe (Figure S5 and S6)

This can be explained as follows. As will be shown in Table 2, the following approximation holds in all solvents where TADF observe: $k_S \gg k_T$, $k_Sk_T \sim k_{isc}k_{risc}$.

The function for the lifetimes is:

(C21) $\tau = \frac{-2}{-(k_S+k_T)\pm\{(k_S+k_T)^2-4(k_Sk_T-k_{isc}k_{risc})\}^{0.5}}$

If we use the approximation:

(C22) $\tau = \frac{-2}{-(k_S+k_T)\pm k_S}$

then:

(C23) $\tau_1 = \frac{1}{k_S}$

and

(C24) $\tau_2 = \frac{2}{k_T}$

Indeed, k_S is independent of oxygen and very large and k_T is strongly dependent on oxygen and very small (explanation for 1 and 2).

The total quantum yield of fluorescence when singlet convert to triplet and vice versa can be think of a sum of quantum yield[3] of prompt fluorescence and quantum yield of delayed fluorescence:

(C25) $\Phi_F = \Phi_{PF} + \Phi_{DF}$

The quantum yield of delayed fluorescence is sum of quantum yields for ISC RISC and fluorescence, ISC RISC ISC RISC and fluorescence and so on.

(C26) $\Phi_{DF} = \Phi_{ISC}\,\Phi_{RISC}\,\Phi_{PF+}\,(\Phi_{ISC}\,\Phi_{RISC})^2\,\Phi_{PF} + (\Phi_{ISC}\,\Phi_{RISC})^3\,\Phi_{PF} + \ldots + (\Phi_{ISC}\,\Phi_{RISC})^n\,\Phi_{PF}$

When n approach infinity.

Meaning equation (C25) can be written as follows:

$\Phi_F = (\Phi_{ISC}\,\Phi_{RISC})^0\Phi_{PF} + (\Phi_{ISC}\,\Phi_{RISC})^1\Phi_{PF+} (\Phi_{ISC}\,\Phi_{RISC})^2\,\Phi_{PF}+(\Phi_{ISC}\,\Phi_{RISC})^3\,\Phi_{PF}+..+(\Phi_{ISC}\,\Phi_{RISC})^n\,\Phi_{PF}$

This is geometric sum equal to:

(C27) $\Phi_F = \Phi_{PF}/1- \Phi_{ISC}\,\Phi_{RISC}$

The only dependence of Φ_F on oxygen concertation is through Φ_{RISC} since the singlet life time is very short and insensitive to oxygen.

We observe that the dominate process from the triplet state is RISC (table 3) so we can approximate Φ_{RISC} as follows:

(C28) $\Phi_{RISC}=k_{RISC}/(k_{RISC}+k_Q[O_2])$

k_Q is the rate of oxygen quenching and $[O_2]$ is oxygen concentration.

From the equations above (C28,C27) it can be seen that the larger the oxygen concentration the smaller Φ_F. In addition, the smaller k_{RISC} is, the smaller Φ_F. in non-polar solvents k_{RISC} is smaller, since the barrier for RISC is higher. In addition, oxygen concentration is higher in non-polar solvents since oxygen is non-polar molecule (explanation for 3).

We can measure the constants B_1, B_2, a_1 and a_2 by fitting the curve of the fluorescence lifetime. Using those constants, we can extract k_S, k_T and $k_{isc}k_{risc}$ (multiplication of the constants). Following the Santos paper,[3] we also extracted the orders of magnitude of k_{isc} and k_{risc} and the multiplication of $\Phi_{ISC}\,\Phi_{RISC}$.

Solvent	$\emptyset_{isc}\emptyset_{risc}(\boldsymbol{O_2})$	$\emptyset_{isc}\emptyset_{risc}(\mathbf{0})$	$\boldsymbol{k_{isc}(ns^{-1})}$	$\boldsymbol{k_{risc}(ns^{-1})}$
Toluene	0.3	0.7	0.1	0.001
Chloroform	0.67	0.73	0.1	0.1
Acetonitrile	0.45	0.56	0.1	0.01
Hexane	-	-	2	-

Table S3. Multiplication of the quantum efficiency for ISC and RISC and estimation of the order of magnitude of ISC and RISC in different solvents

Solvent	$\tau_1(O_2)$ (ns)	$\tau_2(O_2)$ (ns)	$\tau_1(0)$ (ns)	$\tau_2(0)$ (ns)	$k_S(O_2)$ (ns^{-1})	$k_T(O_2)$ (ns^{-1})	$k_S(0)$ (ns^{-1})	$k_T(0)$ (ns^{-1})
Hexane	**0.5**	–	**0.5**	–	**2**	–	**2**	–
Toluene	**2.6**	**103**	**2.8**	**550**	**0.38**	**0.014**	**0.35**	**0.006**
Chloroform	**2.5**	**112**	**2.8**	**165**	**0.38**	**0.026**	**0.34**	**0.021**
Acetonitrile	**2.2**	**65**	**2.4**	**124**	**0.44**	**0.027**	**0.41**	**0.018**

Table S4. Lifetimes and rate constants of each electronic state in different solvents.

From Table S3 it can be understood that ISC and RISC are the main relaxation processes for the singlet and triplet, respectively.

Solvent	$\sigma_{\tau_1(O_2)}$ (ns)	$\sigma_{\tau_2(O_2)}$ (ns)	$\sigma_{\tau_1(0)}$ (ns)	$\sigma_{\tau_2(0)}$ (ns)
Hexane	$6.2 \cdot 10^{-3}$	–	$6.2 \cdot 10^{-3}$	–
Toluene	$2.6 \cdot 10^{-2}$	7.6	$1.6 \cdot 10^{-2}$	4.6
Chloroform	$1.6 \cdot 10^{-2}$	0.59	$1.9 \cdot 10^{-2}$	0.68
Acetonitrile	$1.9 \cdot 10^{-2}$	0.79	$2.2 \cdot 10^{-2}$	1.6

Table S5. standard division of lifetime in different solvents.

S7 Photochemical kinetics

In order to understand whether there is oxygen dependency in the photochemistry of **Bcz** and **F_5BCz**, we monitored their concentration as a function of time with fluorescence. As fluorescence is linear with concentration under small OD conditions, the signal that we get is proportional to the product's concentration. We prepared samples of **Bcz** and **F_5BCz** with very small OD (0.001) so that fluorescence is linear with the concentration and bimolecular processes do not occur. All experiments were done in the fluorimeter under the same conditions and under mixing with a stirrer so that the sample is homogeneous. That is to say, while shining a light on the samples, we measured their fluorescence as function of time. The power of light applied for the photochemical experiments is 0.758mW.

Product(reactant, oxygen)	τ (s)	R^2 (ns)
Carbzaole (BCz,O_2)	324 ± 6	0.996
Carbzaole (BCz,0)	147 ± 2	0.998
Carbzaole (F_5BCz,O_2)	84 ± 3	0.995
Carbzaole (F_5BCz,0)	72 ± 3	0.994
c-F_4BCz (F_5BCz,O_2)	141 ± 7	0.995
c-F_4BCz (F_5BCz,0)	114 ± 3	0.997

Table S6. Lifetime fitted to the fluorescence of the products.

S8 Quantum chemical calculations

Geometry optimizations were performed using density function theory (DFT) (unless otherwise stated). The functional we have chosen is CAM-B3LYP with basis set cc-pVTZ. We chose CAM-B3LYP as the functional because it qualitatively predicted the experimental absorption spectra (Figure S21) and avoids artificial charge transfer state by using range separation. No symmetry restrictions were applied in any of the optimal geometries. The optimal geometries for all structures were confirmed as minima by frequency calculations. No negative frequencies were found for any stationary points presented in this work.

The calculations of the spin orbit coupling matrix element (SOCME) were carried out in the same level of theory as above (TD-DFT/CAM-B3LYP/cc-pVTZ). To estimate the reaction pathways in the singlet excited state and to explore potential singlet/triplet crossings, we have performed a linear interpolation of internal coordinates between two minima geometries. To this end, the geometries were converted to internal coordinates expressed in bonds, bond angle and dihedrals. These internal coordinates were subject to interpolation of 10 geometries between two selected minima structures. These minima structures were either S_0 and S_1 minima (Fig. 1) or S_1 and T_1 minima (Fig. 2).

Geometry optimizations and frequency calculations were carried out with the Gaussian 16[5] program package. The ORCA[4] program was used to calculate the spin orbit coupling matrix elements.

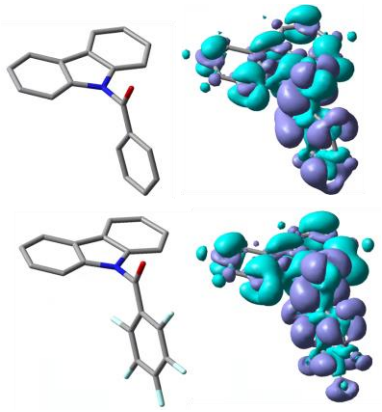

Figure S20. Electron density difference maps and molecular geometries of the S_1 state of **BCz** (top) and **F$_5$BCz** (bottom). Right - Difference in electron density between S_1 and S_0, where turquoise indicates greater electron density in S_0 and purple indicates greater electron density in S_1. The movement of electrons is from turquoise to purple regions – meaning a charge transfer state. Left – Molecular geometry of **BCz** and **F$_5$BCz** in the S_1 state.

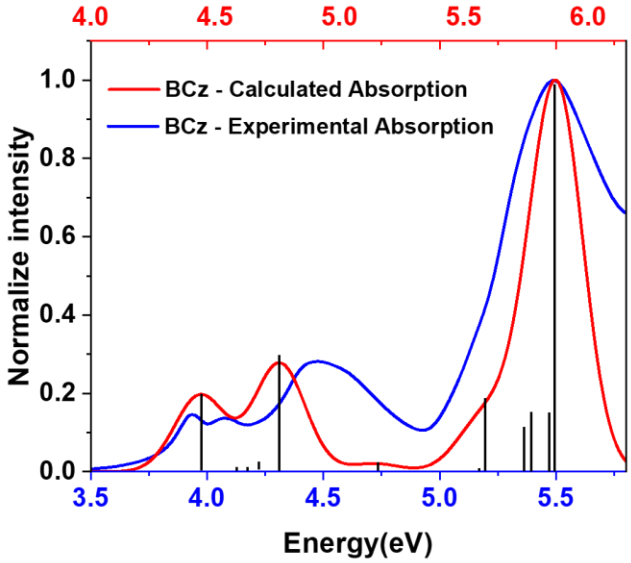

Figure S21. Calculated absorption spectra vs experimental absorption spectra of **BCz**. As can see, the calculated spectrum is hypsochromically shifted by approximately 0.5 eV compared to the experimental spectrum.

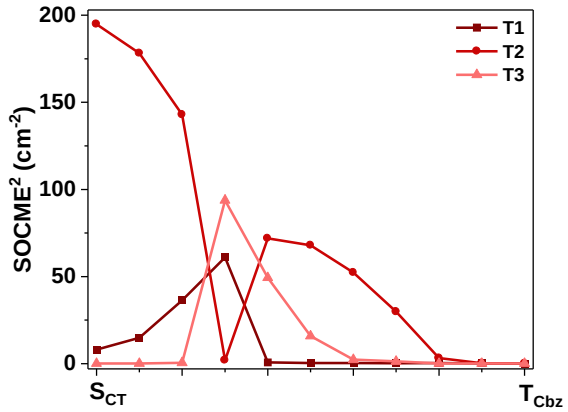

Figure S22. Calculated SOCME between S_1 and T_n. The index n of the triplet states T_n is based on the energetic order at each step of the LIIC between S_1 and T_1 minimum geometries for **BCz**. Level of theory: TD-DFT/CAM-B3LYP/cc-PVTZ.

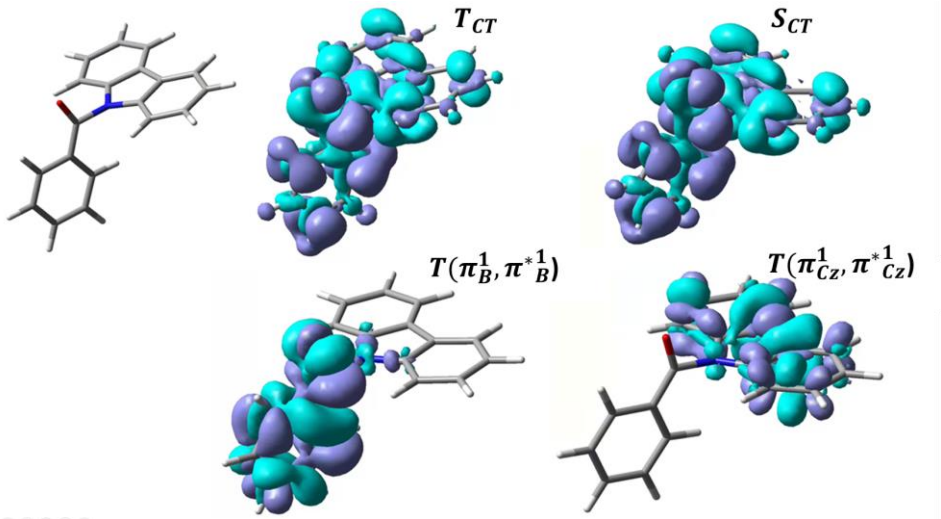

Figure S23. Electron density difference maps of the electronic states from S_1 geometry for **BCz**. Turquoise indicates greater electron density in S_0 and purple indicates greater electron density in excited state.

References:

1 A. Chakrabarti, G. K. Biswas and D. P. Chakraborty, Photo-Fries rearrangements in N-sulphonyl carbazoles, *Tetrahedron*, 1989, **45**, 5059–5064.

2 S. Ghosh, D. B. Datta, I. Datta and T. K. Das, Studies on enamides Part-21:A novel photochemical synthesis of 9H-indolo [3,2,1-de] phenanthridin-9-one, a benzcanthine analogue, *Tetrahedron*, 1989, **45**, 3775–3786.

3 C. Baleizão and M. N. Berberan-Santos, Thermally activated delayed fluorescence as a cycling process between excited singlet and triplet states: Application to the fullerenes, *J. Chem. Phys.*, 2007, **126**, 204510.

4 F. Neese, The ORCA program system, *WIREs Comput. Mol. Sci.*, 2012, **2**, 73–78.

5 Gaussian 09, Revision D.01, M. J. Frisch, G. W. Trucks, H. B. Schlegel, G. E. Scuseria, M. A. Robb, J. R. Cheeseman, G. Scalmani, V. Barone, G. A. Petersson, H. Nakatsuji, X. Li, M. Caricato, A. Marenich, J. Bloino, B. G. Janesko, R. Gomperts, B. Mennucci, H. P. Hratchian, J. V. Ortiz, A. F. Izmaylov, J. L. Sonnenberg, D. Williams-Young, F. Ding, F. Lipparini, F. Egidi, J. Goings, B. Peng, A. Petrone, T. Henderson, D. Ranasinghe, V. G. Zakrzewski, J. Gao, N. Rega, G. Zheng, W. Liang, M. Hada, M. Ehara, K. Toyota, R. Fukuda, J. Hasegawa, M. Ishida, T. Nakajima, Y. Honda, O. Kitao, H. Nakai, T. Vreven, K. Throssell, J. A. Montgomery, Jr., J. E. Peralta, F. Ogliaro, M. Bearpark, J. J. Heyd, E. Brothers, K. N. Kudin, V. N. Staroverov, T. Keith, R. Kobayashi, J. Normand, K. Raghavachari, A. Rendell, J. C. Burant, S. S. Iyengar, J. Tomasi, M. Cossi, J. M. Millam, M. Klene, C. Adamo, R. Cammi, J. W. Ochterski, R. L. Martin, K. Morokuma, O. Farkas, J. B. Foresman, and D. J. Fox, Gaussian, Inc., Wallingford CT, 2016.